

Quantum anomalous Hall effect in atomic crystal layers from in-plane magnetization

Yafei Ren,^{1,2} Junjie Zeng,^{1,2} Xinzhou Deng,^{1,2} Fei Yang,³ Hui Pan,^{3,*} and Zhenhua Qiao^{1,2,†}

¹ICQD, Hefei National Laboratory for Physical Sciences at Microscale, and Synergetic Innovation Center of Quantum Information and Quantum Physics, University of Science and Technology of China, Hefei, Anhui 230026, China

²CAS Key Laboratory of Strongly-Coupled Quantum Matter Physics and Department of Physics, University of Science and Technology of China, Hefei, Anhui 230026, China

³Department of Physics, Beihang University, Beijing 100191, China

(Received 21 December 2015; revised manuscript received 23 July 2016; published 15 August 2016)

We theoretically demonstrate that with *in-plane* magnetization, the quantum anomalous Hall effect (QAHE) can be realized in two-dimensional atomic crystal layers with preserved inversion symmetry but broken out-of-plane mirror reflection symmetry. By taking the honeycomb lattice system as an example, we find that the low-buckled structure satisfying the symmetry criteria is crucial to induce QAHE. The topologically nontrivial bulk gap carrying a Chern number of $\mathcal{C} = \pm 1$ opens in the vicinity of the saddle points M , where the band dispersion exhibits strong anisotropy. We further show that the QAHE with electrically tunable Chern number can be achieved in Bernal-stacked multilayer systems, and the applied interlayer potential differences can dramatically decrease the critical magnetization to make the QAHE experimentally feasible.

DOI: 10.1103/PhysRevB.94.085411

I. INTRODUCTION

The quantum anomalous Hall effect (QAHE), manifesting itself as quantized Hall conductance and vanishing longitudinal conductance, has attracted broad interest recently [1]. In analogy to the quantum Hall effect from strong out-of-plane magnetic field, the QAHE has been intensively studied by introducing out-of-plane ferromagnetism in various systems, such as topological insulator thin films [1–6], quantum wells [7,8], and atomic crystal layers, e.g., honeycomb-lattice systems [1,9–14]. Experimentally, by using ferromagnetic insulating substrates, the AHE has been reported in graphene, though much effort is still required to realize the quantized counterpart [15–18]. In such systems, a weak magnetic field is usually required to align the system magnetization that prefers in-plane orientation. This inspires us to consider whether it is possible to produce QAHE from *in-plane* magnetism. So far, except limited studies in quantum-well structures [7,8], the QAHE from in-plane magnetization has not been reported in two-dimensional (2D) atomic crystals.

Starting from symmetry analysis, we investigate the possibility of realizing QAHE from in-plane magnetization in atomic crystal layers and show that QAHE can occur when the inversion symmetry is preserved but the out-of-plane mirror-reflection symmetry is broken. We show that the QAHE cannot form in a planar honeycomb lattice, e.g., graphene, but can be realized in *low-buckled* honeycomb lattices such as silicene. With an in-plane magnetization, the topologically nontrivial bulk gap hosting the QAHE with a Chern number of $\mathcal{C} = \pm 1$ opens around M points, the saddle points with strong anisotropy. This is different from other QAHE systems from out-of-plane magnetization with band-gap opening at isotropic Dirac points [1,8,9,12–14,19]. We further show that in multilayer systems, high Chern numbers can be achieved and tuned via electric means. The application of vertical

electric field can dramatically decrease the lowest critical magnetization, make the QAHE experimentally feasible.

II. SYSTEM HAMILTONIAN

The tight-binding Hamiltonian of a monolayer low-buckled honeycomb lattice with in-plane magnetization can be expressed as [12,13]

$$H = -t \sum_{\langle ij \rangle} c_i^\dagger c_j + i t_{\text{I}} \sum_{\langle\langle ij \rangle\rangle} v_{ij} c_i^\dagger s_z c_j - i t_{\text{IR}} \sum_{\langle\langle ij \rangle\rangle} \mu_{ij} c_i^\dagger (s \times \hat{\mathbf{d}}_{ij})_z c_j + \lambda \sum_i c_i^\dagger \hat{\mathbf{m}} \cdot s c_i, \quad (1)$$

where $c_i^\dagger = (c_{i\uparrow}^\dagger, c_{i\downarrow}^\dagger)^T$ is the creation operator for an electron at the i th site with \uparrow and \downarrow representing spin-up and -down states. The first term stands for the nearest-neighbor hopping with an amplitude of t , and the second term is the intrinsic spin-orbit coupling (SOC), where $v_{ij} = \mathbf{d}_i \times \mathbf{d}_j / |\mathbf{d}_i \times \mathbf{d}_j|$ with $\mathbf{d}_{i,j}$ being the two nearest bonds connecting next-nearest-neighbor sites. These two terms correspond to the Hamiltonian of a planar honeycomb lattice with preserved mirror-reflection symmetry (i.e., $z \rightarrow -z$). This symmetry can be broken in the low-buckled structure, which is reflected by the intrinsic-Rashba SOC H_{IR} displayed as the third term where $\mu_{ij} = \pm 1$ for A/B sublattices, s are spin-Pauli matrices, and $\hat{\mathbf{d}}_{ij}$ is a unit vector from site j to i . The last term represents the in-plane magnetization, with the strength and orientation, respectively, being λ and $\hat{\mathbf{m}} = (\cos \phi, \sin \phi, 0)$.

III. SYMMETRY ANALYSIS

We begin from the symmetry analysis of the Hamiltonian and corresponding Berry curvature $\Omega_n(\mathbf{k}) = \Omega_n^z(\mathbf{k}) \hat{z}$ based on the anomalous velocity in the presence of in-plane electric field \mathbf{E} [20,21],

$$\mathbf{v}_n(\mathbf{k}) = \frac{\partial \varepsilon_n(\mathbf{k})}{\hbar \partial \mathbf{k}} - \frac{e}{\hbar} \mathbf{E} \times \Omega_n(\mathbf{k}). \quad (2)$$

*Corresponding author: hpan@buaa.edu.cn

†Corresponding author: qiao@ustc.edu.cn

TABLE I. Parity of in-plane (out-of-plane) magnetization H_{\parallel} (H_{\perp}), intrinsic (extrinsic) Rashba SOC H_{IR} (H_{ER}), staggered AB sublattice potentials H_{AB} , velocity \mathbf{v} , momentum \mathbf{k} , and electric field \mathbf{E} under the symmetric operations of time reversal \mathcal{T} , out-of-plane mirror reflection \mathcal{M}_z , and inversion \mathcal{I} . $+/-$ indicates even/odd parity. See more details of each term in the Supplemental Material [21].

	H_{\parallel}	H_{\perp}	H_{IR}	H_{ER}	H_{AB}	\mathbf{v}	\mathbf{k}	\mathbf{E}
\mathcal{T}	-	-	+	+	+	-	-	+
\mathcal{M}_z	-	+	-	-	+	+	+	+
\mathcal{I}	+	+	+	-	-	-	-	-

The integration of $\Omega_n^z(\mathbf{k})$ over the first Brillouin zone gives the Chern number that characterizes the topological property of the n th band [20,22]. We focus on the operations of inversion \mathcal{I} , time reversal \mathcal{T} , and out-of-plane mirror reflection \mathcal{M}_z (i.e., $z \rightarrow -z$). Under these operations, the parities of velocity \mathbf{v} , momentum \mathbf{k} , and electric field \mathbf{E} are listed in Table I. We first consider a planar honeycomb lattice with vanishing intrinsic-Rashba SOC, which is invariant under these three operations. In this consideration, the introduction of in-plane magnetization, which has odd parities under both \mathcal{T} and \mathcal{M}_z operations and even parity under inversion \mathcal{I} , cannot break the invariance of the system under the joint operation of $\mathcal{T} \otimes \mathcal{M}_z \otimes \mathcal{I}$. The preservation of this symmetry gives vanishing $\Omega_n^z(\mathbf{k})$ [21].

To generate nonzero Berry curvature, the joint symmetry of $\mathcal{T} \otimes \mathcal{M}_z \otimes \mathcal{I}$ must be broken. One potential approach is to break the inversion symmetry \mathcal{I} by introducing staggered sublattice potential H_{AB} [21], which, however, is invariant under the operation of $\mathcal{T} \otimes \mathcal{M}_z$. This requires that $\Omega_n^z(\mathbf{k})$ is an odd function of momentum \mathbf{k} , and results in a vanishing Chern number [21,23]. Therefore, one can conclude that the symmetries of the system under both $\mathcal{T} \otimes \mathcal{M}_z \otimes \mathcal{I}$ and $\mathcal{T} \otimes \mathcal{M}_z$ should be simultaneously broken to induce nonzero Chern number. We find that this symmetry criteria can be satisfied by introducing intrinsic-Rashba SOC in the low-buckled structures, which is odd under \mathcal{M}_z while invariant under the inversion \mathcal{I} operation. Thus, its combination with in-plane magnetization as shown in Eq. (1) breaks both symmetries of $\mathcal{T} \otimes \mathcal{M}_z$ and $\mathcal{T} \otimes \mathcal{M}_z \otimes \mathcal{I}$, leading to nonzero Berry curvature that is an even function of momentum. Therefore, nonzero Berry-curvature integration may lead to QAHE in insulator and AHE in metal. These analyses are consistent with that in Ref. [23].

In addition to the intrinsic-Rashba SOC, the extrinsic-Rashba SOC H_{ER} from structural inversion asymmetry, e.g., from the substrate, also has the odd parity under mirror-reflection \mathcal{M}_z . However, different from the intrinsic one, it is odd under inversion \mathcal{I} operation. Therefore, its combination with in-plane magnetization preserves the joint symmetry of $\mathcal{T} \otimes \mathcal{M}_z \otimes \mathcal{I}$, leading to zero Berry curvature. In contrast to the in-plane one, the out-of-plane magnetization itself breaks both the joint symmetries of $\mathcal{T} \otimes \mathcal{M}_z \otimes \mathcal{I}$ and $\mathcal{T} \otimes \mathcal{M}_z$ simultaneously. Thus, together with either intrinsic- or extrinsic-Rashba SOC, it can lead to nonzero Berry curvature, which is an even function of \mathbf{k} guaranteed by the invariance under the operation of either \mathcal{I} or $\mathcal{M}_z \otimes \mathcal{I}$ [9,13]. Such differences between in-plane and out-of-plane magnetizations in symmetry clearly distinguish our proposed mechanism from

other reported ones. Below, we numerically demonstrate the QAHE from in-plane magnetization in low-buckled honeycomb lattice.

IV. MONOLAYER SYSTEM

We first calculate the band structure with the magnetization orientation being $\phi = \pi/6$ [21]. At $\lambda = 0$, a band gap opens at valleys K/K' [see Fig. 1(a)], harboring a 2D \mathbb{Z}_2 topological insulator [24]. When a nonzero magnetization $\lambda < t$ is applied, the doubly degenerate bands become split into two species, as highlighted in blue and red, which are characterized by different band gaps Δ_1 and Δ_2 , as displayed in Fig. 1(b). This insulating phase with broken time-reversal symmetry is topologically trivial with $\mathcal{C} = 0$ [20–22] and an absence of gapless edge modes [Fig. 1(g)]. When the magnetization reaches a critical value of $\lambda = t$, the band gap Δ_1 is nearly unchanged while Δ_2 is closed at M points, as displayed in Fig. 1(c). For even larger magnetization strength, e.g., $\lambda > t$, the degeneracy at the saddle points M is lifted and the band gap Δ_2 reopens, which changes the Berry-curvature distribution, as shown in Fig. 1(f). One can find that the Berry curvature is negative for M_1 and M_3 , but positive for M_2 giving rise to a negative Chern number $\mathcal{C} = -1$, indicating the formation of QAHE. This can be further confirmed by the emergence of chiral gapless edge modes (in red), as displayed in Fig. 1(h).

We further study the dependence of the topological phase on the magnetization orientation. Figure 2(a) displays the band gap as well as the corresponding topological phases in the m_x - m_y plane with $(m_x, m_y) = \lambda(\cos \phi, \sin \phi)$. The white dot denotes the \mathbb{Z}_2 topological insulator phase at $\lambda = 0$. For $\lambda < t$, the insulating phase with vanishing Chern number $\mathcal{C} = 0$ occurs, independent of magnetization orientation. The increase of magnetization drives the band-gap closing at $\lambda = t$, but reopening for $\lambda > t$ to host QAHE characterized by Chern numbers of $\mathcal{C} = \pm 1$, as labeled in Fig. 2(a) [9,21]. Different from the case of $\lambda < t$, the reopened band gap is strongly dependent on the magnetization orientation ϕ and vanishes at $\phi = n\pi/3$ ($n = 0-5$), as highlighted by dashed lines separating QAHEs with opposite Chern numbers of $\mathcal{C} = \pm 1$. This dependence of Chern number on ϕ is consistent with the symmetry analysis in Refs. [7] and [25].

Here, we stress that the intrinsic-Rashba SOC in the *low-buckled* structure plays an important role in reopening the band gap Δ_2 . As shown in Fig. 2(b), the amplitude of the intrinsic SOC is momentum dependent and vanishes at high-symmetric lines connecting Γ and M points, as denoted by purple dashed lines. In the absence of intrinsic-Rashba SOC, this feature leads to the formation of Dirac points at Γ - M lines whenever the magnetization $\lambda > t$. Thus, the QAHE cannot form without intrinsic-Rashba SOC. To better demonstrate this finding, the low-energy effective Hamiltonians around M points are provided as

$$\begin{aligned}
 h_{M_1}(\mathbf{q}, \phi) &= +[m\sigma_z + a\sigma_x + b(\phi)\sigma_y], \\
 h_{M_2}(\mathbf{q}, \phi) &= -[m\sigma_z + a\sigma_x + b(\phi + \pi/3)\sigma_y], \\
 h_{M_3}(\mathbf{q}, \phi) &= -[m\sigma_z + a\sigma_x + b(\phi - \pi/3)\sigma_y],
 \end{aligned} \tag{3}$$

where the unit of momentum is set to be $1/\sqrt{3}a_0$, with a_0 being the nearest-neighbor distance. $\sigma_{x,y,z}$ are Pauli matrices

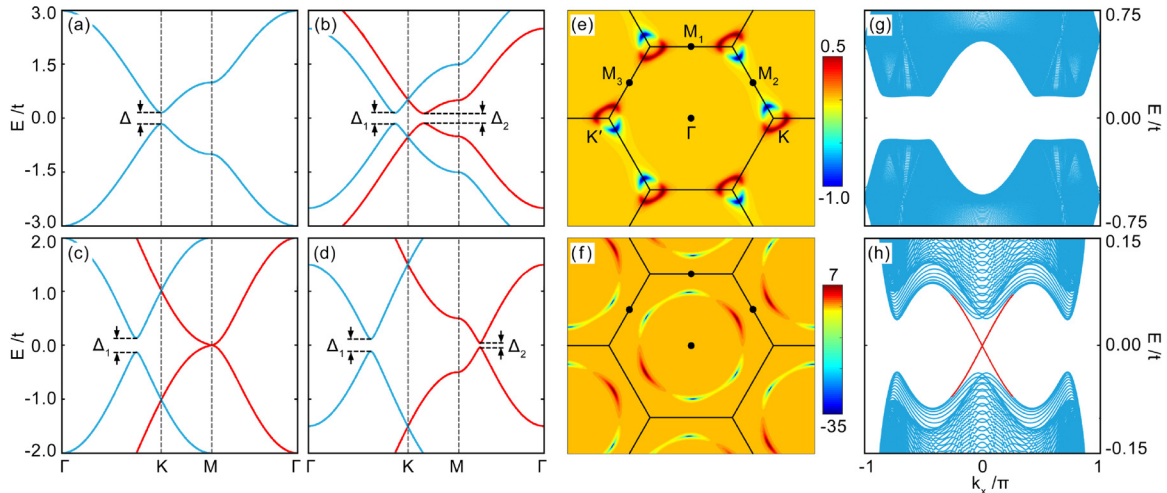


FIG. 1. (a)–(d): Band structures of low-buckled honeycomb lattice in the presence of different in-plane magnetization strengths of $\lambda/t =$ (a) 0.0, (b) 0.5, (c) 1.0, and (d) 1.5 at the orientation of $\phi = \pi/6$. With the increase of λ , a topological phase transition occurs accompanied by a bulk band-gap (c) closing and (d) reopening. (e),(f) Berry-curvature distribution in the Brillouin zone for the insulating states shown in (b) and (d). (g),(h) The corresponding zigzag-ribbon band structures for the systems shown in (b) and (d). (f) Red lines highlight the chiral gapless modes of the QAHE. In our calculations, the SOC parameters are chosen to be $t_I = t_{IR} = 0.03t$.

and the mass term $m = -\delta\lambda + t(3q_y^2 - q_x^2)/4$ shows strong anisotropic momentum dependence on $\delta\lambda = \lambda - t$. $a = 4q_x t_I$ and $b = t_{IR}(3q_y \sin\phi - q_x \cos\phi)$ are separately contributed from intrinsic and intrinsic-Rashba SOC parameters giving rise to x and y components of the spin texture [21]. In the absence of either term, the band gap cannot reopen when $\delta\lambda > 0$. Moreover, without intrinsic-Rashba SOC, the angular dependence disappears since the angle ϕ is related to t_{IR} . It is noteworthy that in our systems considered, the symmetry, anisotropy, and the angle-dependent Chern number carried by each M point [21] are completely different from those reported previously [2,9,19].

V. MULTILAYER SYSTEMS

So far, we have shown that the in-plane magnetization-induced QAHE can be formed in a low-buckled monolayer

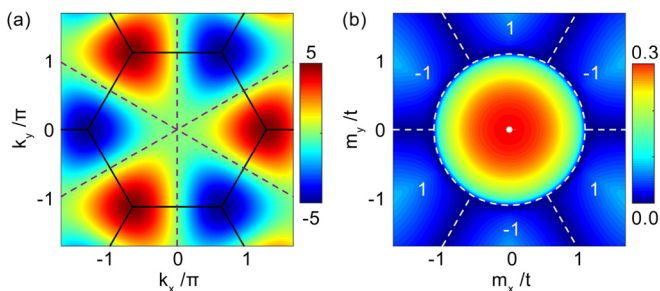


FIG. 2. (a) Phase diagram of the low-buckled honeycomb lattice with $(m_x, m_y) = \lambda(\cos\phi, \sin\phi)$. The white dot at the center indicates the 2D \mathbb{Z}_2 topological insulator at $\lambda = 0$. When $0 < \lambda < t$, the system is a trivial insulator. When $\lambda > t$, the system is a QAHE with alternating Chern numbers $\mathcal{C} = \pm 1$. Dashed lines indicate the phase boundaries. (b) Contour plot of the amplitude of intrinsic SOC in momentum space. The first Brillouin zone is denoted by solid lines, and the intrinsic SOC vanishes along dashed lines. In our calculation, the SOC parameters are chosen to be $t_I = t_{IR} = 0.03t$.

honeycomb-lattice system. However, a daunting challenge for realizing this QAHE is the extremely large magnetization that is comparable to the hopping energy t . Below, we show that the lowest critical magnetization for realizing QAHE can be dramatically decreased in multilayer systems. Let us first take the bilayer system as an example and adopt the same SOC parameters as those in monolayer cases [21]. We display the bulk band structures for different λ and ϕ , and find that the band gap shows the same angular dependence as that of the monolayer system [see Fig. 3(a)]. The band gap also closes at $M_{1,2,3}$ points when topological phase transitions occur [21]. However, different from a monolayer system, additional topological phases with Chern numbers of $\mathcal{C} = \pm 2$ arise. Moreover, a topological phase transition from $\mathcal{C} = 0$ to $\mathcal{C} = \pm 1$ appears at the critical magnetization $\lambda_{C1} \simeq 0.8t$, which is smaller than that in the monolayer case.

The presence of layer degree of freedom allows that λ_{C1} can be further reduced by applying an interlayer potential difference U via an electric field. As displayed in Fig. 3(b), we find that the increase of U can dramatically decrease the critical magnetization λ_{C1} , while correspondingly enlarges λ_{C2} that separates the topological phases of $\mathcal{C} = \pm 1$ and ± 2 . Therefore, the QAHE with $\mathcal{C} = \pm 1$ can be achieved at a rather smaller magnetization in the presence of a sizable electric-field strength. In addition, the dependence of $\lambda_{C1,2}$ on interlayer potential difference also makes it possible to realize the QAHE with electrically tunable Chern numbers. The inset of Fig. 3(b) shows that the topological phase transitions are independent of the amplitudes of SOC parameters.

The cases for Bernal-stacked multilayer systems are similar to those in the bilayer one. As highlighted by solid lines in Fig. 3(c), large-Chern-number QAHEs appear for n -layer systems as the magnetization λ increases with an upper limit of $\mathcal{C} = n$. When U is applied, the critical magnetization is decreased (increased) for small- (large-)Chern-number QAHEs [see dashed lines in Fig. 3(c)]. For λ_{C1} , the lowest magnetization to induce the QAHE with $\mathcal{C} = \pm 1$, we find that

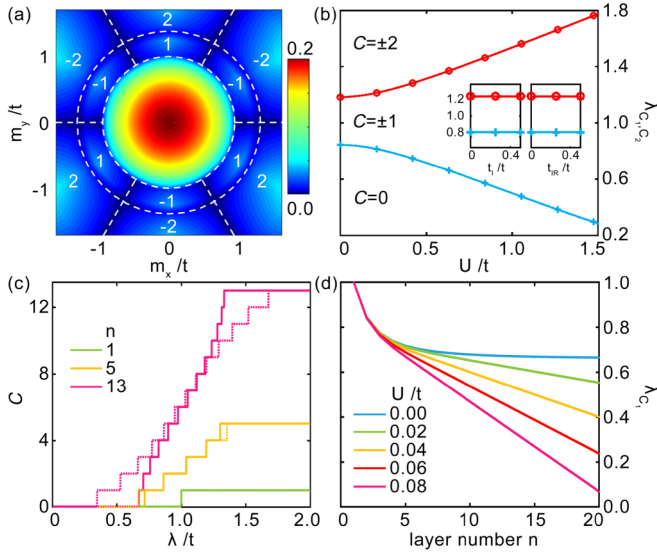


FIG. 3. (a) Phase diagram of the bilayer low-buckled honeycomb lattice in the m_x - m_y plane. Dashed lines indicate the phase boundaries. Chern numbers are labeled in the QAHE regions accordingly. (b) Evolution of critical phase boundaries λ_{C_1, C_2} as a function of the interlayer potential difference. (c) Chern number \mathcal{C} as a function of the amplitude of magnetization λ at fixed $\phi = -\pi/6$ for different layers. Solid and dashed curves correspond to $U = 0$ and $U = 0.05t$, respectively. (d) The lowest critical magnetization amplitude to induce the QAHE of $\mathcal{C} = \pm 1$ as a function of the layer number n at fixed $\phi = -\pi/6$ for different potential differences. In our calculation, the SOC's are chosen to be $t_l = t_{\text{R}} = 0.03t$.

it decreases slowly as the layer thickness increases for $U = 0$, as shown by the light blue line in Fig. 3(d). When U gradually increases, λ_{C_1} can be greatly decreased for multilayer systems, as illustrated in Fig. 3(d). These findings strongly indicate that a multilayer low-buckled honeycomb-lattice system under proper electric field is a more ideal and more experimentally feasible platform to realize the in-plane magnetization-induced QAHE.

VI. SUMMARY AND DISCUSSIONS

In this paper, by using symmetry analysis, we have theoretically revealed that in 2D systems, nonzero Chern number can only occur in systems with broken symmetries of $\mathcal{T} \otimes \mathcal{M}_z \otimes \mathcal{I}$ and $\mathcal{T} \otimes \mathcal{M}_z$. Both symmetries can be simultaneously broken by the out-of-plane magnetization, while preserved by the in-plane one. This makes the QAHE from in-plane magnetization only possible in systems with certain constraints, such as the atomic crystal layers with preserved inversion symmetry but broken mirror-reflection symmetry. Such differences between in-plane and out-of-plane magnetizations in symmetry distinguish our proposed QAHE mechanism from the previous ones. We numerically verified the realization of QAHE in low-buckled honeycomb lattice, where the band gap hosting the QAHE opens in the vicinity of

time-reversal symmetric M points exhibiting strong anisotropy and harbors magnetization-orientation-dependent noninteger Chern number.

Experimentally, the in-plane magnetization could be introduced by applying an in-plane magnetic field that cannot form Landau levels in the ultrathin films or proximately coupling with ferromagnetic insulating substrates [15,16], where a symmetric setup with the low-buckled honeycomb-lattice system sandwiched by two identical ferromagnetic insulating layers is required to eliminate the influence of extrinsic-Rashba SOC that is detrimental to the QAHE from in-plane magnetization [21]. However, the extremely large magnetization strength required, i.e., $\lambda_{C_1} = t$, makes the experimental realization of the QAHE in a monolayer system difficult. There are two possible ways to overcome this difficulty. One is to decrease the nearest-neighbor hopping energy t by, e.g., constructing an artificial organometallic material with low-buckled honeycomb structure, where the effective nearest-neighbor hopping energy t is relatively weak and the exchange field is rather strong and can even be much larger than t [26]. The other one is to consider Bernal-stacked multilayer systems, where the critical magnetization λ_{C_1} gradually decreases along with the increase of system thickness and could be further dramatically reduced by applying interlayer potential differences via a vertical electric field. Our studies together with the recent experimental realization of Bernal-stacked multilayer silicene [27–30] strongly suggest the QAHE from in-plane magnetization could be experimentally achievable in such system with a perpendicular electric field.

Apart from the half-filled low-buckled honeycomb lattice (e.g., silicene, germanene, and stanene), there are plenty of atomic crystal layers satisfying the symmetry criteria discussed above, such as organometallic materials, bismuth bilayer, black and blue phosphorene [1]. The QAHE from in-plane magnetization may also be realized in these systems and their hybridized structures, where the magnetization required may be small enough to be experimentally feasible. Furthermore, such symmetry analysis on Berry curvature is not limited to QAHE. With nonzero Berry curvature that is an even function of momentum, the AHE is also expected in a metallic system with in-plane magnetization.

ACKNOWLEDGMENTS

We are grateful to Professor Q.-F. Sun for valuable discussions. This work is financially supported by the China Government Youth 1000-Plan Talent Program, Anhui Provincial Natural Science Foundation, National Natural Science Foundation of China (Grants No. 11574019 and No. 11474265), Fundamental Research Funds for the Central Universities (Grants No. WK351000001 and No. WK2030020027), and the National Key R & D Program (Grant No. 2016YFA0301700). The supercomputing center of USTC is gratefully acknowledged for the high-performance computing assistance.

[1] For recent reviews on QAHE, see H. Weng, R. Yu, X. Hu, X. Dai, and Z. Fang, *Adv. Phys.* **64**, 227 (2015); C.-X. Liu, S.-C. Zhang, and X.-L. Qi,

Annu. Rev. Condens. Matter Phys. **7**, 301 (2016); Y. F. Ren, Z. H. Qiao, and Q. Niu, *Rep. Prog. Phys.* **79**, 066501 (2016).

- [2] R. Yu, W. Zhang, H. J. Zhang, S.-C. Zhang, X. Dai, and Z. Fang, *Science* **329**, 61 (2010).
- [3] C.-Z. Chang, J. Zhang, X. Feng, J. Shen, Z. Zhang, M. Guo, K. Li, Y. Ou, P. Wei, L.-L. Wang, Z.-Q. Ji, Y. Feng, S. Ji, X. Chen, J. Jia, X. Dai, Z. Fang, S.-C. Zhang, K. He, Y. Wang, L. Lu, X.-C. Ma, and Q.-K. Xue, *Science* **340**, 167 (2013).
- [4] J. G. Checkelsky, R. Yoshimi, A. Tsukazaki, K. S. Takahashi, Y. Kozuka, J. Falson, M. Kawasaki, and Y. Tokura, *Nat. Phys.* **10**, 731 (2014).
- [5] X. Kou, S. T. Guo, Y. Fan, L. Pan, M. Lang, Y. Jiang, Q. Shao, T. Nie, K. Murata, J. Tang, Y. Wang, L. He, T.-K. Lee, W.-L. Lee, and K. L. Wang, *Phys. Rev. Lett.* **113**, 137201 (2014).
- [6] C. Z. Chang, W. Zhao, D. Y. Kim, H. Zhang, B. A. Assaf, D. Heiman, S.-C. Zhang, C. Liu, M. H. W. Chan, and J. S. Moodera, *Nat. Mater.* **14**, 473 (2015).
- [7] X. Liu, H. C. Hsu, and C. X. Liu, *Phys. Rev. Lett.* **111**, 086802 (2013).
- [8] Y. Zhang and C. Zhang, *Phys. Rev. B* **84**, 085123 (2011).
- [9] Z. Qiao, S. A. Yang, W. X. Feng, W. K. Tse, J. Ding, Y. Yao, J. Wang, and Q. Niu, *Phys. Rev. B* **82**, 161414(R) (2010).
- [10] W.-K. Tse, Z. Qiao, Y. Yao, A. H. MacDonald, and Q. Niu, *Phys. Rev. B* **83**, 155447 (2011).
- [11] Z. Qiao, H. Jiang, X. Li, Y. Yao, and Q. Niu, *Phys. Rev. B* **85**, 115439 (2012).
- [12] M. Ezawa, *Phys. Rev. Lett.* **109**, 055502 (2012).
- [13] H. Pan, Z. Li, C.-C. Liu, G. Zhu, Z. Qiao, and Y. Yao, *Phys. Rev. Lett.* **112**, 106802 (2014).
- [14] M. Ezawa, *Phys. Rev. B* **87**, 155415 (2013).
- [15] Z. Qiao, W. Ren, H. Chen, L. Bellaiche, Z. Zhang, A. H. MacDonald, and Q. Niu, *Phys. Rev. Lett.* **112**, 116404 (2014).
- [16] J. Zhang, B. Zhao, Y. Yao, and Z. Yang, *Sci. Rep.* **5**, 10629 (2015).
- [17] G. Cheng, L. Wei, L. Cheng, H. Liang, X. Zhang, H. Li, G. Yu, and C. Zeng, *Appl. Phys. Lett.* **105**, 133111 (2014).
- [18] Z. Wang, C. Tang, R. Sachs, Y. Barlas, and J. Shi, *Phys. Rev. Lett.* **114**, 016603 (2015).
- [19] F. D. M. Haldane, *Phys. Rev. Lett.* **61**, 2015 (1988).
- [20] D. Xiao, M.-C. Chang, and Q. Niu, *Rev. Mod. Phys.* **82**, 1959 (2010).
- [21] See Supplemental Material at <http://link.aps.org/supplemental/10.1103/PhysRevB.94.085411> for detailed derivation of the proposed QAHE formation mechanism.
- [22] D. J. Thouless, M. Kohmoto, M. P. Nightingale, and M. den Nijs, *Phys. Rev. Lett.* **49**, 405 (1982).
- [23] H. Chen, Q. Niu, and A. H. MacDonald, *Phys. Rev. Lett.* **112**, 017205 (2014).
- [24] C.-C. Liu, W. Feng, and Y. Yao, *Phys. Rev. Lett.* **107**, 076802 (2011).
- [25] C. Fang, M. J. Gilbert, and B. A. Bernevig, *Phys. Rev. B* **86**, 115112 (2012).
- [26] Z. F. Wang, Z. Liu, and F. Liu, *Phys. Rev. Lett.* **110**, 196801 (2013).
- [27] J. Chen, Y. Du, Z. Li, W. Li, B. Feng, J. Qiu, P. Cheng, S. X. Dou, L. Chen, and K. Wu, *Sci. Rep.* **5**, 13590 (2015).
- [28] H. Fu, L. Chen, J. Chen, J. Qiu, Z. Ding, J. Zhang, K. Wu, Hui Li, and S. Meng, *Nanoscale* **7**, 15880 (2015).
- [29] K.-H. Wu, *Chin. Phys. B* **24**, 086802 (2015).
- [30] Z. Li, J. Zhuang, L. Chen, Y. Du, X. Xu, L. Wang, X. Pi, X. Wang, K. Wu, and S. X. Dou, [arXiv:1509.01975](https://arxiv.org/abs/1509.01975).